CHAPTER–4B

Bis(pyridyl)-di-imines as Naked Eye Colorimetric Fluorescence Sensor for Fe(II) Ions

Bis(pyridyl)-di-imines as Naked Eye Colorimetric Fluorescence Sensor for Fe(II) Ions

4B.1 Introduction

Chemical, biological, industrial, and environmental processes are profoundly affected by transition metal ions.[1] Nowadays, different types of the sensors have been developed for detecting transition metals.[2] Out of the various transition metals, there is a frequent need to detect Fe(II) and Fe(III) as iron being one of the essential elements for life. Its deficiency or surplus can lead to adverse effects to the mankind in particular and to our biosphere as a whole. Excess of iron in our body causes hemochromatosis and Alzheimer's disease, while its deficiency results in anemia, liver diseases, kidney damages and hypoferrimia.[3] Environmental pollution related due to several iron smelting industries creates imbalance of iron, which further leads to significant hazards to the biological system and by the way to overall environment. There is a need to control of iron concentration level in human cells and for that there is a requirement of detecting its presence.

Most of the methods used to detect iron by Schiff base receptors were mainly based on fluorescence due to the responsive photophysical behaviour of the Schiff bases. Fluorescence techniques are usually cost effective, has high selectivity and fast sensing approach compared to other sensing methods.[4] Compared to other transition metals, there are few reports in literature related to sensing of iron. Another challenge is the detection of Fe(II), if the time duration of sensing is more, then during sensing it can easily get oxidized to Fe(III). From biological perspective,[5] it is necessary to develop fluorescent based sensor to detect Fe(II) selectively. Wu et al., have synthesized a multifunctional Schiff base receptor that acted as a fluorescence sensor for detecting Fe(II) selectively.[6] In addition to that, the receptor also showed a colorimetric response for Fe(II) and was also able to detect F^- ions. Cheal Kim group designed an imidazole-based Schiff base compound which acted as a fluorescent sensor for Al(III) and Zn(II) and also as a colorimetric chemosensor for Fe(III) and Fe(II) ions with a detection limit of 7.4 μM for Fe(II) and 6.8 μM for Fe(III).[7] This group has further prepared another Schiff base compound which was found to have a selective colorimetric sensing ability towards iron.[8] Fe(II) sensors have developed based on the property, such as electrochemiluminescence Cu-MOF,[9] sol-gel based optical sensor,[10] potential chemical sensor incorporating 1,10-phenanthroline.[11] These are shown good limit of detection. Very recently Cu-MOF (metal organic framework) has been explored as Fe(II) sensor with detection limit of 4×10^{-11} M via enhancement of electrochemiluminescence property in the system. The sol-gel based optical sensor is used to prepare the biosensor. 2,4,6-tris(2-pyridyl)- -s-triazine

organic indicator dye has shown as sol-gel optical sensor for Fe(II) determination up to 5-115 ng mL^{-1}. 1,10-phenanthroline is another organic dye used for Fe(II) determination through spectrophotometric technique. Recently, phenanthroline was used on the mesoporous silica nanospheres scaffold and acted as colorimetric potential chemical sensor for evaluating the corrosion level of Fe(II) in boiler water system.

Sensing of Fe(II) in biological systems is still challenging as one of the major problem is the selectivity of receptors in sensing Fe(II) only in presence other metal ions. There are present two types of Fe(II) sensors in literature based on the photophysical property: (1) 'Fluorescent Turn off' and (2) 'Fluorescent Turn on'.[12] Calcein,[2c] and Phen Green SK[13] have shown the fluorescent turn off response for Fe(II) ion. RhoNox-1[14]and Iron Probe-1[12] have shown the fluorescent turn on response for Fe(II) ion. The ratiometric fluorescent Fe(II) sensor has also synthesized first time by Tang group[15] for living cell imaging to visualize the labile Fe(II). Later FRET (Fluorescence resonance energy transfer) based ratiometric fluorescence probe has been prepared for cell imaging through introducing the labile Fe(II) ion by Chang group's. Calcein dye was used for Fe(II) sensing in intracellular system via degradation of calcein through Fe(II) complex formation with rate constant 3×10^5 M^{-1} S^{-1}.[16] It is also used as fluorescent chemosensor[17] for determination of low molecular weight of iron in serum.

Parsaee et al., have reported DFT calculations on a novel phenothiazine Schiff base compound and its copper complex for optimization, molecular orbital (MO) determination, Mülliken population analysis (MPA), the contour of electrostatic potential (ESP) and molecular electrostatic potential (MSP) map. The calculations fully supported the formation of chemically stable copper complex and finally leading to a rationale for the enhancement of the antibacterial activity of compounds. DFT calculation that was carried out B3LYP levels of theory with double basis set LANL2DZ for copper and 6311+G (d,p) basis set for others atoms.[18] Lopez et al., have optimized the four organotin Schiff base complexes through DFT calculation at the restricted B3LYP level with a 631G(d) basis set.[19] The theoretical HOMO-LUMO gap is in agreement with the experimental HOMO-LUMO analyzed by cyclic voltammetry. Arroudj et al., have determined the HOMO-LUMO energy gap (E_g), the electric dipole moment (μ), the polarizability (α) and the first hyperpolarizability (β) of Schiff base molecule using DFT calculation B3LYP method with LANL2DZ basis set and all those results are well agreement with the observed second-order nonlinear optical properties.[20] Mossalamy et al., have synthesized three Schiff base charge-transfer complexes of aryl 2-azomethine

dibenzothiophene and HOMO-LUMO energy gap estimated using B3LYP/SDD method corresponds to the charge transfer complexes.[21] Hasan Tanak has reported a dimethyl phenyl-based Schiff base, which shows keto-enol tautomerism and nonlinear optical properties. The analysis was verified by theoretical DFT calculation using B3LYP/6-311++G(d,p) level.[22] Rastogi et al., have correlated anti-wear properties of three salicylaldehyde based Schiff base compound with iron metal surfaces by the various parameters like frontier molecular orbital energy, HOMO-LUMO orbitals and Mülliken charges, which were obtained from B3LYP/6-311++(d,p) method.[23] There are accomplished DFT study on several Schiff base molecule and their complexes (Figure 4B.1).[24]

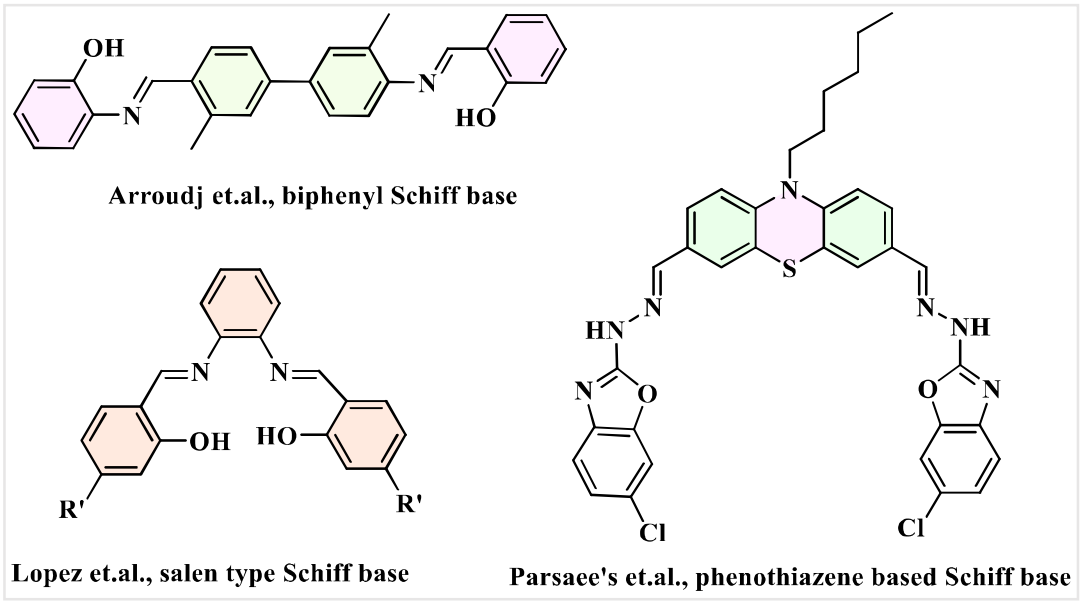

Figure 4B.1: Different Schiff base moieties[18,19,20] used for complexation through DFT calculation

In this chapter, we have reported an application of (1E,1'E)-N,N'-(ethane-1,2-diyl)bis(1-(pyridin-2-yl)methanimine), **L2c**, acted as naked eye colorimetric fluorescence quencher chemosensor, highly selective for Fe(II) ion (Scheme 1). This is first time reporting to **L2c** act as a sensor for Fe(II), which is very easily synthesized as compared to other substantial cost-effective sensors. Applications of **L2c** was reported previously by other groups as a ligand to metal charge transfer Fe(III) complex[25] and in metal extraction.[26] Previously, our group has reported photophysical properties of **L2c** [27] and their structural correlation and butane diamine sensor for Ni(II) and Cd(II)[28] (chapter 4A). The binding constant, binding mode and limit of detection of Fe(II) with **L2c** were determined experimentally by using the mole ratio method **L2c** and its probable complex with Fe(II) were done to obtain the frontier molecular orbitals to rationalize the observed Fe(II) sensing behaviour of **L2c**.

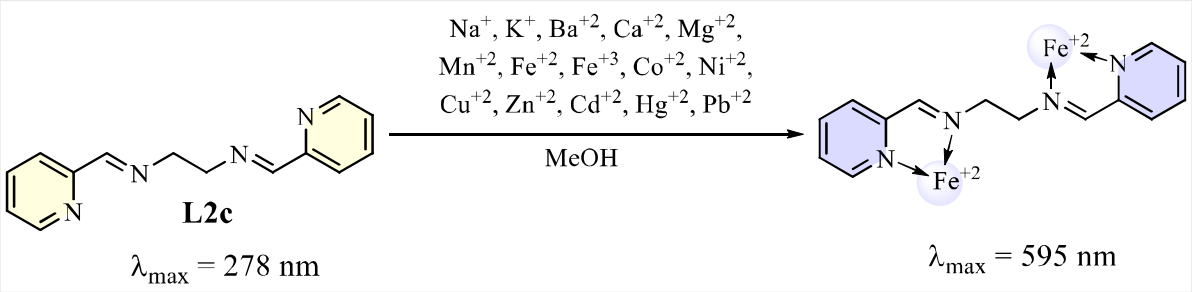

Scheme 4B.1: *(*Proposed*)* Metal ion sensing property of **L2c**

4B.2 Experimental

4B.2.1 General

FTIR, UV-visible and Fluorescence spectra were recorded using ABB Bomen MB-3000, Shimadzu UV-2450 and Fluorimax-4 0426C0809 spectrometers, respectively. Proton and Carbon-13 Nuclear Magnetic Resonance (^{1}H NMR and ^{13}C NMR) spectra were recorded on a Bruker Avance III (400 MHz) instrument. Powder X-Ray Diffraction (XRD) data was collected with Rigaku miniflex II, λ =1.54, Cu Kα.

4B.2.2 (1E,1'E) -*N, N'*- (Butane-1,4-diyl)bis(1-(pyridin-2-yl)methanimine) (L2c)

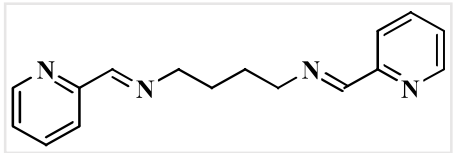

L2c was synthesized by the usual method of preparation of Schiff bases[29], which involved the condensation reaction of primary diamines with an aldehyde precursor in alcoholic solution under reflux conditions. Yield: 42%; Melting point: 66 ºC; IR (cm^{-1}, KBr pellet): 3047(s), 3009(w), 2916(s), 2885(vs), 2831(s), 1643(vs), 1566(vs), 1466(vs), 1427(vs), 1335(vs), 1296(s), 1219(s), 1041(vs), 972(vs), 918(vs), 864(vs), 771(vs) (Figure A-99). ^{1}H NMR (400 MHz, $CDCl_3$) δ 8.64 (ddd, *J* = 4.9, 1.8, 1.0 Hz, 2H), 8.44 (s, 2H), 8.00 (dt, *J* = 7.9, 1.1 Hz, 2H), 7.79 – 7.71 (br, 2H), 7.32 (ddd, *J* = 7.5, 4.9, 1.2 Hz, 2H), 4.09 (br, 4H). (Figure A-100). ^{13}C NMR (100 MHz, $CDCl_3$) δ ppm: 163.37, 154.27, 149.33, 136.49, 124.71, 121.29, 61.26 (Figure A-101).

4B.2.3 DFT computations

Gaussian-09 programme package was used for performing all DFT calculations. For optimizing the structures of **L2c** and **Fe(II)-L2c** complex, we used B3LYP levels of theory with basis set 6-311G++(d,p) for **L2c**, double basis set 6-311G*+(2d,p) for iron atom and 6-31G*+(d) for other atoms.

4B.3 Results and discussion

4B.3.1 Colorimetric response of L2c towards Fe (II) analyzed by photophysical studies

L2c has shown absorption maxima at 234 nm ($\pi \rightarrow \pi^*$) and 278 nm ($n \rightarrow \pi^*$) in UV-visible absorption spectrum. To detect the sensitivity of **L2c** towards various metal ions, UV- visible spectra of **L2c** in presence of a series of metal salts (NaCl, KCl, $MgNO_3$, $CaCl_2$, $BaCl_2$, $MnCl_2$, $FeSO_4$, $Fe(NO_3)_3$, $Co(NO_3)_2$, $Ni(NO_3)_2$, $Cu(NO_3)_2$, $Zn(NO_3)_2$, $CdCl_2$, $Pb(NO_3)_2$, $HgCl_2$) in 1:2 ratio (**L2c**:metal salt) were recorded. No significant change (intensity or shift) in absorption spectra of mixtures (Figure 4B.2) was observed for alkali and alkaline earth metals, however, all the d-block metals showed interaction with **L2c**. Fe(II)-**L2c** mixture gave unique spectral pattern with absorbance peak in the visible region (yellow) at 595 nm, hump at 503 nm and another peak at 372 nm.

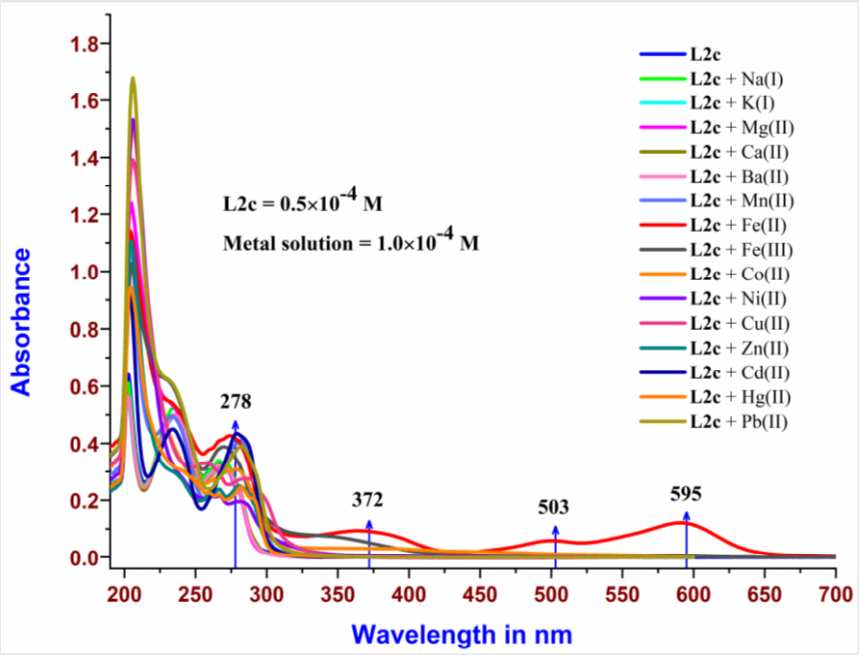

Figure 4B.2: UV-Visible absorption spectra of **L2c** with different metal salts in 1:2 ratio

4B.3.2 Turn off fluorescence response of L2c towards Fe(II) investigated through photoluminescence (PL) analysis in presence of other metal ions

The emission spectra of **L2c** (0.5×10^{-4} M) in the presence of above studied metal ions mixed in **L2c** to metal ion ratio 1:2 were recorded for excitation wavelengths 370 and 410 nm. The PL spectra of **L2c** with alkali metals showed enhancement of intensity while that of transition metal ions showed a quenching effect. But the PL spectra of **L2c** in presence of Fe(II) showed unique features. Interaction of Fe(II) with **L2c** showed the appearance of three peaks have appeared when the excitation wavelength was at 410 nm and 370 nm. Also, the quenching

effect appeared in the PL of **L2c** due to Fe(II) was much more than any other transition metal ions. Similar to the colorimetric observation of Fe(II) interaction with **L2c**, Co(II) and Ni(II) have also shown a colour change in the visible region when the excitation wavelength is in the visible region. While keeping the excitation wavelength in the UV-visible region, Mn(II) has shown dark yellow emission and Fe(II) has shown faint blue emission. These PL spectra give an idea about the fact that most of the metal ions are interacting with **L2c**, but an effective colorimetric response is observed in the case of Fe(II) ions (Figure 4B.3).

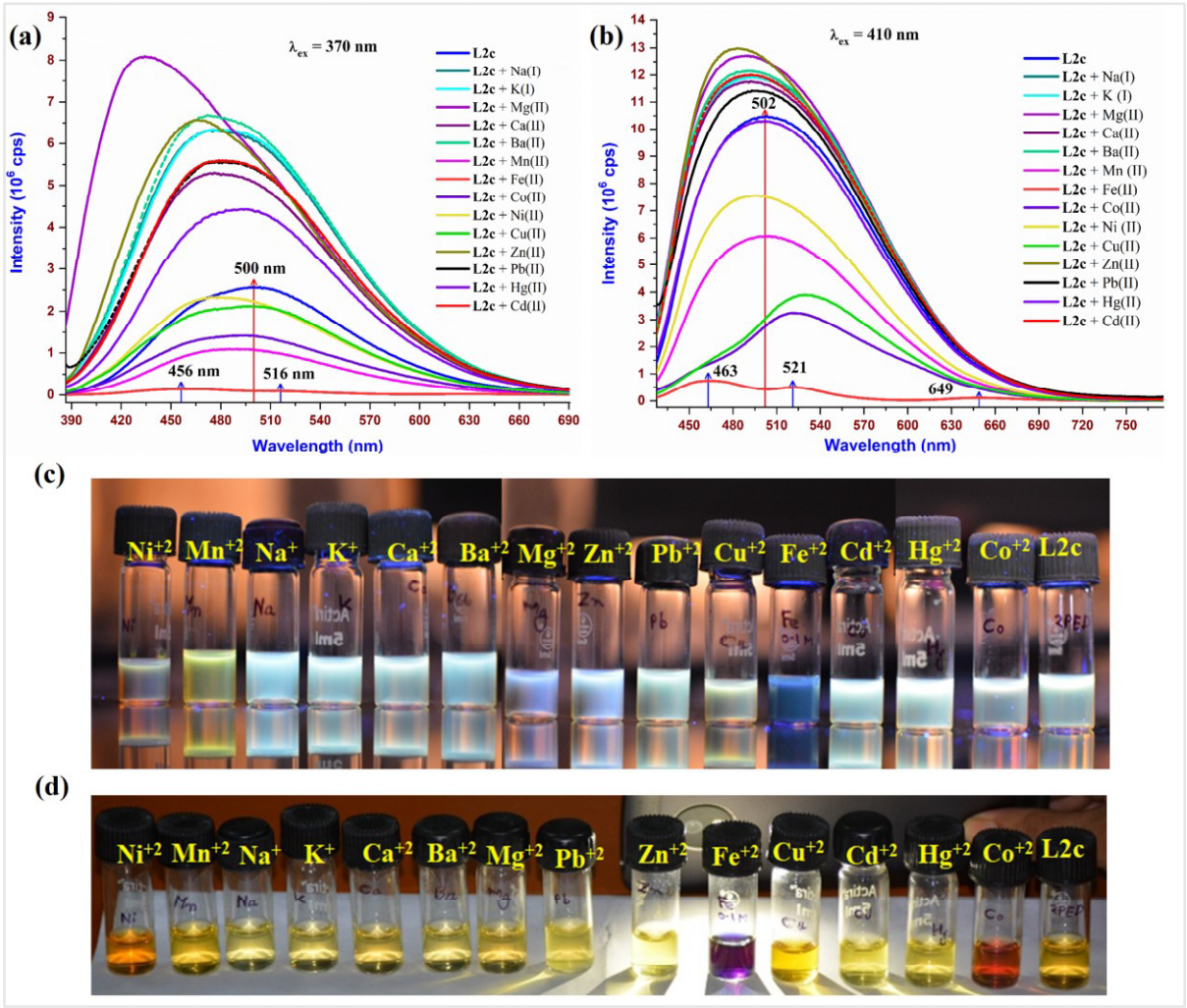

Figure 4B.3: (a and b) PL spectra of **L2c** with different metal ions at two different excitation wavelengths. (c) Under UV-visible light (365 nm) and (d) Visible light

4B.3.3 Analysis of the Fe(II)-L2c interaction

The binding of Fe(II) with **L2c** is also visible to the naked eye by instant appearance of dark purple colour. Mole ratio and Yoe-Jones methods have been used to determine the binding ratio and association constant. For this, **L2c** solution in methanol (1 mL; 0.5×10^{-4} M) was

titrated with methanolic $FeSO_4$ solution (1×10^{-3} M) (Figure 4B.4a) and UV-visible spectrum was recorded after each addition of 10 μL of Fe(II) solution. A linear increase in the absorbance corresponding to the peak at 595 nm was observed upon addition of Fe(II) solution until volume reached 100 μL. At this point, maximum absorbance was recorded and no apparent change in the absorbance was observed on further increasing Fe(II) concentration. The saturation in absorbance is shown in linear fit plot of Absorbance (at λ = 595 nm) vs. Volume of Fe(II) solution which is equivalent to 1.05×10^{-4} M of Fe(II) (Figure 4B.4b). From this saturation point, the binding ratio of ligand to metal was determined as 1:2.1 (~ 1:2).

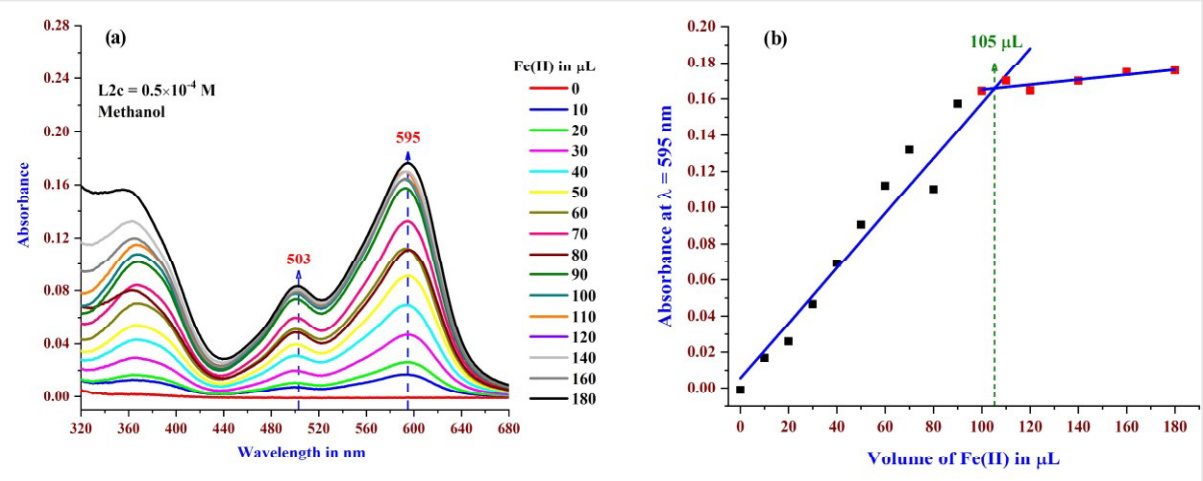

Figure 4B.4:(a) UV-Visible absorption spectra for titration of **L2c** (1 mL; 0.5 x 10^{-4} M) with of Fe(II) solution of solution (1 x 10^{-3} M) in 10 μL steps (Total volume of solution = 2mL), (b) Piece wise linear fit plot of Absorbance (at 595 nm peak) vs. Volume of Fe(II) solution plot

Yoe Jones method was applied on absorbance data at 595 nm to determine the binding constant of Fe(II) with **L2c** using a nonlinear square fit analysis method. The binding constant, *K* is found to be 7.2 x 10^{10} M^{-2} for Fe^{2+} (Figure 4B.5). The limit of detection was done by measuring the absorbance of different concentrations of Fe(II) in 1×10^{-5} M of **L2c**. The calculation part is done from the plot of Absorbance (at 595 nm) vs. Conc. of Fe(II), the detection limit was calculated as 25 μM for Fe(II) (Figure A-102).

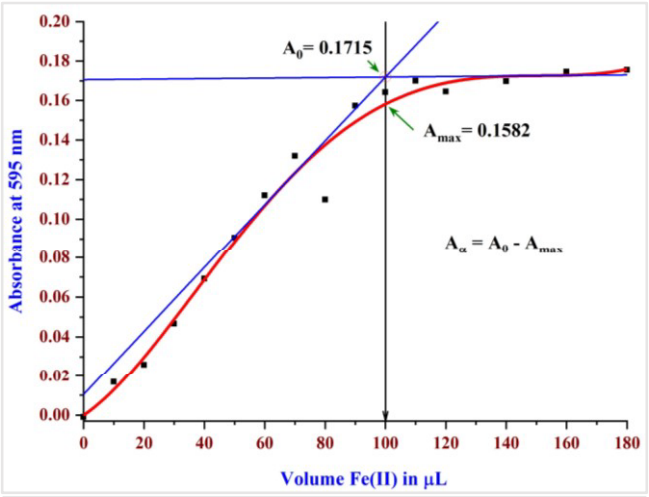

Figure 4B.5: Determination of binding constant of Fe(II) with **L2c** from Yoe Jones method using non-linear least square fit analysis method at 595 nm

4B.3.4 Interference of other metal ions

As **L2c** is interacting with various metal ions, we have determined the competence of Fe(II) for **L2c** over other metal ions through UV-visible absorbance study. For this methanolic solution of **L2c** was mixed with the methanolic solution containing both Fe(II) and other metal ion and absorbance spectra were recorded (Figure A-103a). From the absorbance data at 595 nm (Figure 4B.6), it was evident that interference during the sensing of Fe(II) with **L2c** due to most of the tested metal ions is within 15% except for Mg(II), Pb(II), Ni(II), Mn(II) and Cd(II).

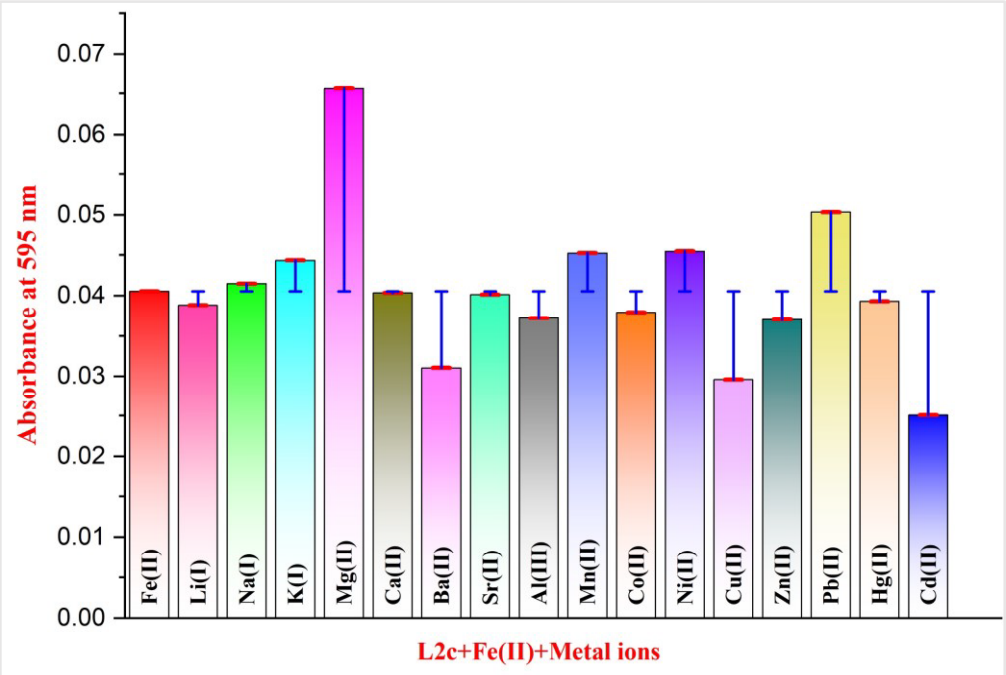

Figure 4B.6: Variation of absorbance at wavelength 278 nm by adding different metal ions

4B.3.5 Effect of anions in Fe(II)-L2c complex

The effect of the presence of various anions such as OH^-, NO_3^-, N_3^-, ClO_4^-, Cl^- and BF_4^- on the **Fe(II)-L2c** complex was tested by taking 50 µL of 10^{-3} M of each anion solution and adding to 100 µL of 10^{-3} M of the **Fe(II)-L2c** solution in methanol (final volume 3 ml). It was observed that except for Cl^- anion, other anions did not affect the absorbance at 595 nm corresponding to **Fe(II)-L2c** (Figure 4B.7a). The addition of Cl^- resulted in the quenching of the absorbance at 595 nm.

4B.3.6 Effect of pH on Fe(II)-L2c complex

The study of pH sustainability of **Fe(II)-L2c** was performed in a wide range of pH in aqueous HEPES [(4-(2-hydroxyethyl)-1-piperazineethanesulfonicacid)] buffer solution (Methanol/HEPES, 1:1, v/v, pH = 7.3) (Figure A-103b). In this regard, 5 mL of 1 mM of

HEPES solution was taken to prepare a buffer solution of different pH by adding H_2SO_4/NaOH. The absorbance of **Fe(II)-L2c** was measured for each pH by adding 1 ml of buffer solution of the corresponding pH to a solution of 1ml of 50 µL of Fe (II) and 25 µL of **L2c** methanolic solution, while the total volume was fixed at 2 mL. Figure 4B.7b shows that the absorbance intensity of **Fe(II)-L2c** is not influenced by any change in the pH in the range of 5-10. Within this pH range, **L2c** could be effectively used for sensing Fe(II) both in environmental as well as in biological samples.

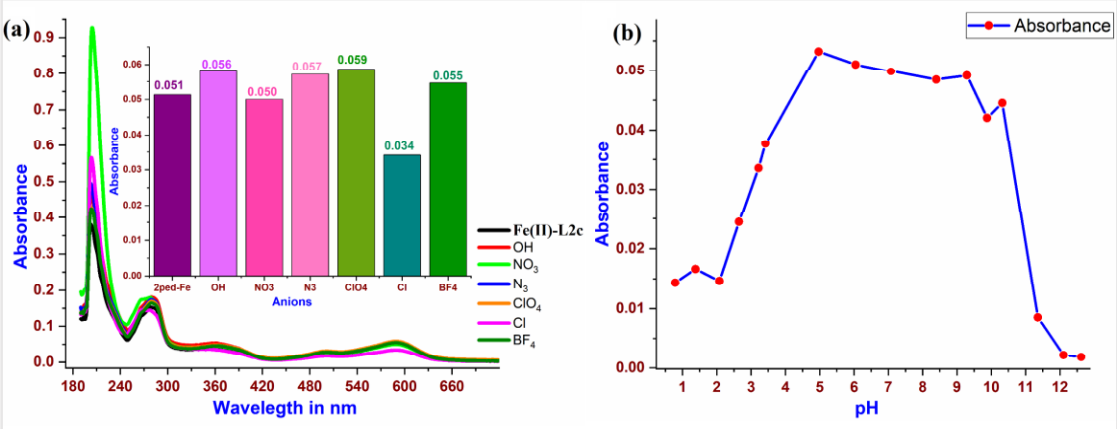

Figure 4B.7: (a) The UV-visible spectra and the bar diagram represents the Reversibility of **Fe(II)-L2c** towards anions at 595 nm (b) Absorbance (at 595 nm) for probe-Fe^{+2} complex solution at different pH values taken in the MeOH/ aqueous HEPES buffer solution (1:1, v/v, 1 mM, pH = 7.3)

4B.3.7 Fe(II)-L2c complexation study by NMR analysis

The complexation of **L2c** with Fe(II) was analyzed by ^{1}H NMR, wherein 0.3 mL of **L2c** solution (0.01 M) in $CDCl_3$ was mixed with 0.3 mL of Fe(II) solution (0.02 M) in $CDCl_3$ and recorded the NMR spectra. ^{1}H NMR of free **L2c** has five types of protons in the aromatic region (Figure 4B.8), where CH protons adjacent to pyridine nitrogen (**a)** appear at 8.64 ppm as a doublet of doublet of doublet, while imine CH protons (**e**) appear as a singlet at 8.44 ppm. The ^{1}H NMR of **L2c** on complexation with Fe(II) result no change in the peak position, however showed the diamagnetic nature of the metal ion which is being complexed with **L2c**. This supports the fact that Fe ion present in the complex has +2 oxidation state and is low spin, otherwise, the paramagnetic effect would have resulted in broadening of peaks in the NMR.

4B.3.8 Rationalizing the photophysical observation of L2c in presence of Fe(II) using theoretical calculations

Gaussian 09 programme package used for performing all DFT calculations. For optimization of **L2c** and **Fe(II)**-**L2c** complex, B3LYP levels of theory with basis set 6311G(d,p) for **L2c**,

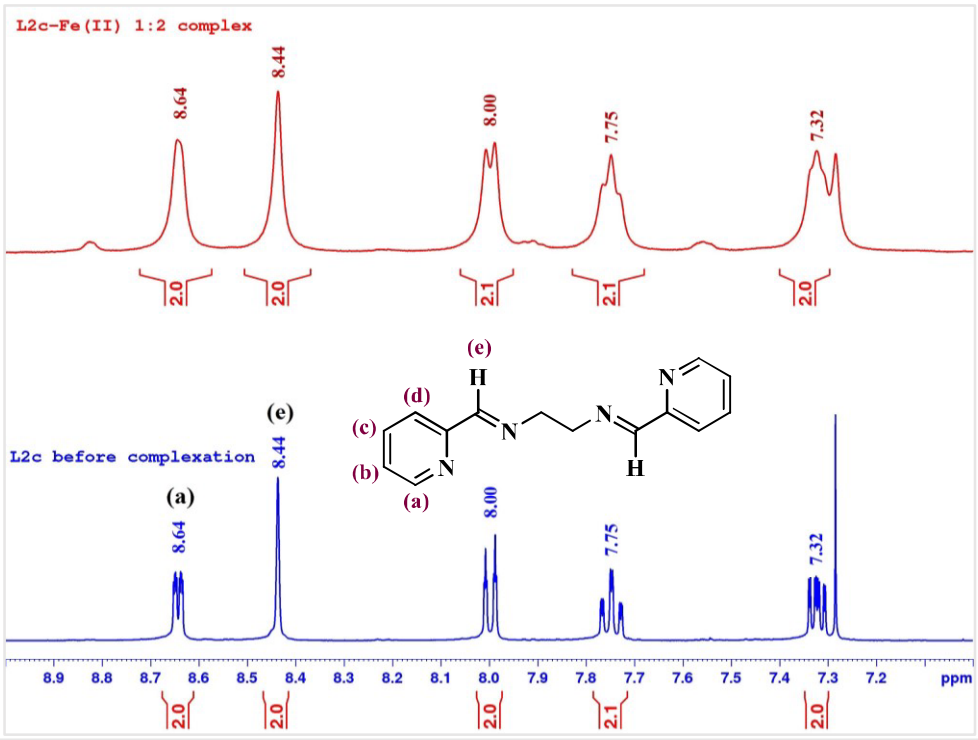

Figure 4B.8: NMR spectra of Fe(II)- **L2c** complex and **L2c** receptor

double basis set 6-311+G*(2d,p) for iron atom and 631+G*(d) for other atoms respectively, were used.

4B.3.8.1 Optimization of L2c

The optimized geometry of **L2c** showed marked differences as compared to the single-crystal structure of **L2c**, which is reported elsewhere (Figure 4B.9). The major difference lies in the torsion angle across N-C-C-N bond; in optimized geometry, the torsion angle is 180° while in the crystal structure, the torsion angle is -73.06°. It is quite evident that the geometry of **L2c** in the single crystal structure is a result of the overall packing of the molecules due to various non-covalent interactions while the optimized geometry only one molecule has taken into

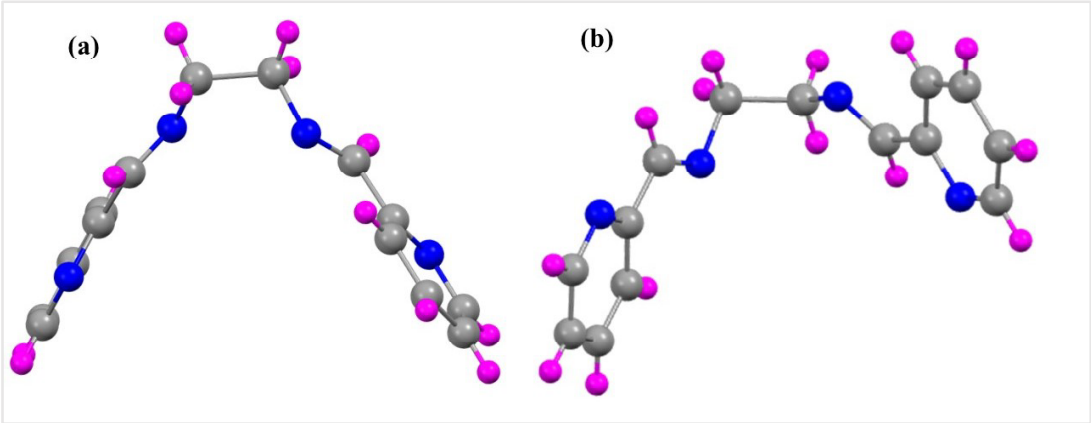

Figure 4B.9: (a) Crystal structure of **L2c** and (b) Optimized structure of **L2c**

account and did not consider effect of neighbouring molecules. The stabilization energy in the case of the optimized geometry of **L2c** was found to be -761.06389 Hartrees. The energy of the HOMO (63) level is -6.80257 eV and that of the LUMO (64) level is -1.70289 eV. The net HOMO-LUMO gap (E_g) is +5.09968 eV. It was also found that the electron density of HOMO is spread over the C=N region and pyridyl nitrogen. While in LUMO, the electron density is spread over the entire molecule that represents in Figure 4B.11. The frontier molecular orbitals calculations on the optimized geometry of **L2c** suggested it to be a highly electron rich moiety

4B.3.8.2 Elucidation of the geometry of Fe(II)-L2c Complex

As the structure of **L2c** with Fe(II) is not known to us, four possible geometries of **Fe(II)-L2c** complex were suggested with different basis set with charge state 4 (as 1:2 ratio of **L2c**: Fe(II)) and the spin multiplicity 1 due to low spin state of Fe(II) (Table 4B.1). The calculations show that the most stable structure corresponds to **Fe(II)- L2c12**, where the stabilization energy is calculated to be –3898.59736 Hartrees. The geometry corresponding to this most stabilized structure showed that the two imine nitrogens are coordinates to the Fe(II) center while the remaining coordinating sites are satisfied by water molecules (Figure 4B.10a). The bond lengths and bond angles are shown in Table 4B.2.

After rationalizing this data, it was suggested that the optimized geometry of **Fe(II)-L2c** complex may have a distorted octahedral geometry, where two pyridyl rings are positioned in

Table 4B.1: DFT calculation table for receptor and **Fe(II)-L2c** complexes

Molecule	Functional	Basis set		Charge	Spin Multiplicity	Energy (A.U)	HOMO-LUMO gap (eV)
		CHN	Fe				
L2c2 (gas phase)	B3LYP	6-311++G (d,p)	-	0	1	-761.06389	5.09968
L2c2ccdc2 (gas phase)	B3LYP	6-311++G (2d,p)	-	0	1	-761.112	5.2085
L2c ccdc2ml (methanol)	B3LYP	6-311++G (2d,p)	-	0	1	-761.1234	5.1821
Fe-**L2c**12 (gas phase)	B3LYP	6-31+G* (d)	6-311+G (2d,p)	4	1	-3898.59736	3.943
Fe-**L2c**6 (gas phase)	B3LYP	6-31G (d)	6-311+G	4	1	-3898.5494	3.8923
Fe-**L2c**7 (gas phase)	B3LYP	6-31G+ (d,p)	6-311+G (2d,p)	4	1	-3898.2730	3.6232
Fe-**L2c**10 (gas phase)	B3LYP	6-31G+ (d)	6-311+G*	4	1	-3898.2717	3.6263

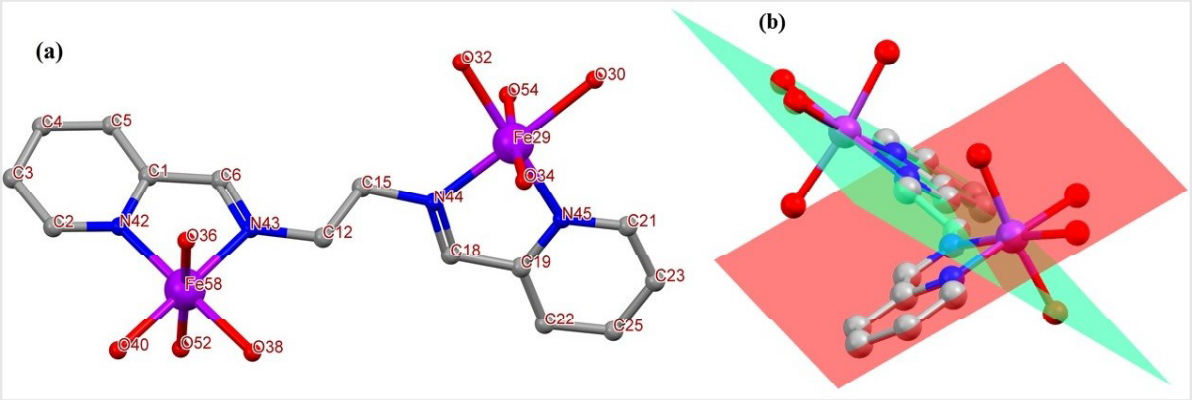

Figure 4B.10: (a) Optimized geometry of **Fe(II)-L2c** complex (b) Two Fe(II) are lying in two different planes

Table 4B.2: The bond lengths and bond angles of **Fe(II)–L2c12**

Bond length	Bond angle
N_{42}-Fe_{58} = 1.986Å	∠$O_{36}Fe_{58}N_{42}$ = 45.07°
N_{43}-Fe_{58} = 2.037 Å	∠$O_{36}Fe_{58}N_{43}$ = 95.92°
Fe_{58}-O_{40} = 2.088 Å	∠$O_{36}Fe_{58}O_{40}$ = 82.72°
Fe_{58}-O_{38} = 2.075 Å	∠$O_{40}Fe_{58}O_{52}$ = 91.14°
Fe_{58}-O_{36} = 2.045 Å	∠$N_{42}Fe_{58}O_{52}$ = 92.43°
Fe_{58}-O_{52} = 2.051 Å	∠$N_{42}Fe_{58}O_{38}$ = 176.17°

a trans manner with respect to ethyl spacer (Figure 4B.11b). The imine bond length is 1.300 Å. The torsion angle N-C-C-N is 179.06°. It was found that in the HOMO, the electron cloud is delocalized on two Fe(II) centers along with imine nitrogen orbitals while in LUMO, the electron cloud is located on two pyridyl rings. As was noted previously, the HOMO of free **L2c** showed electron distribution over the entire molecule, but after complexation, the electron density has shifted to the Fe(II) center, which can be viewed as a ligand to metal charge transfer (LMCT). High values of HOMO (Figure 4B.11 and Table A-8) represent that a molecule can donate an electron to a perfect acceptor. Our receptor is electron rich with a high value of HOMO-LUMO gap compared to that of the HOMO-LUMO gap of iron complexes (Figure 4B.11). Analysis of the frontier molecular orbitals suggested that the charge distribution goes through receptor to iron centres.

4B.3.8.3 The theoretical UV-visible calculation

The ground state geometry of **L2c** was optimized with n state 40 at TD-CPCM B3LYP level of theory with a basis set 6-311++g (2d,p) in methanol solvent. It has revealed two maxima in UV-visible spectrum, 276 nm, and 210 nm with oscillator strength f_{osc} = 0.4978 and f_{osc} =

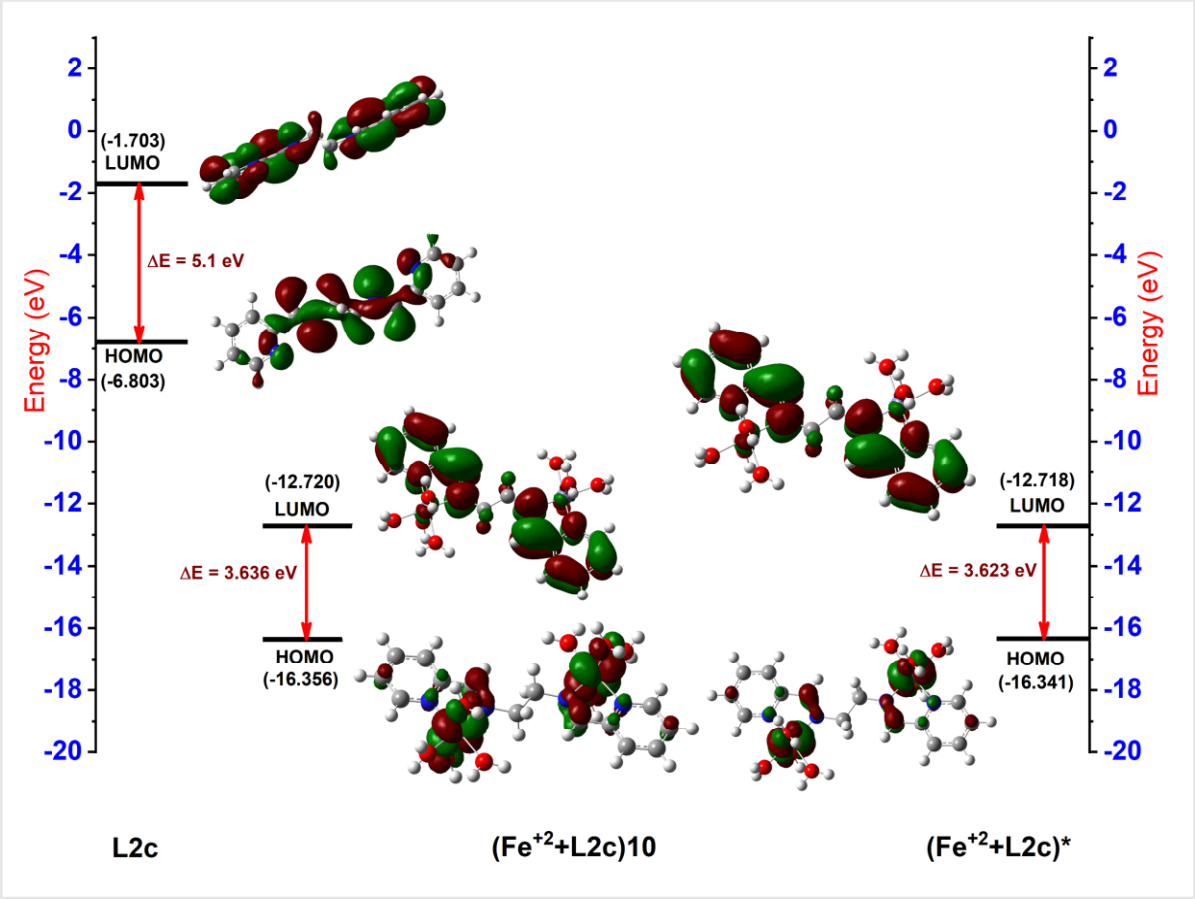

Figure 4B.11: Contour molecular orbitals of receptor and **Fe(II)-L2c** with HOMO-LUMO gap

0.0778, which nearly matches with the experimentally observed 278 nm and 235 nm (Figure 4B.12a). This absorbance corresponds to the n $\rightarrow \pi^*$ and $\pi \rightarrow \pi^*$ of the pyridine moiety of the ligand. The theoretical electronic absorption spectra of **Fe(II)-L2c** were measured by the TD-DFT method based on the B3LYP/6-311++G(d,p) level optimized structure of **Fe(II)-L2c** complex in methanol (Figure 4B.12b) which nearly closer to the experimental λ values.

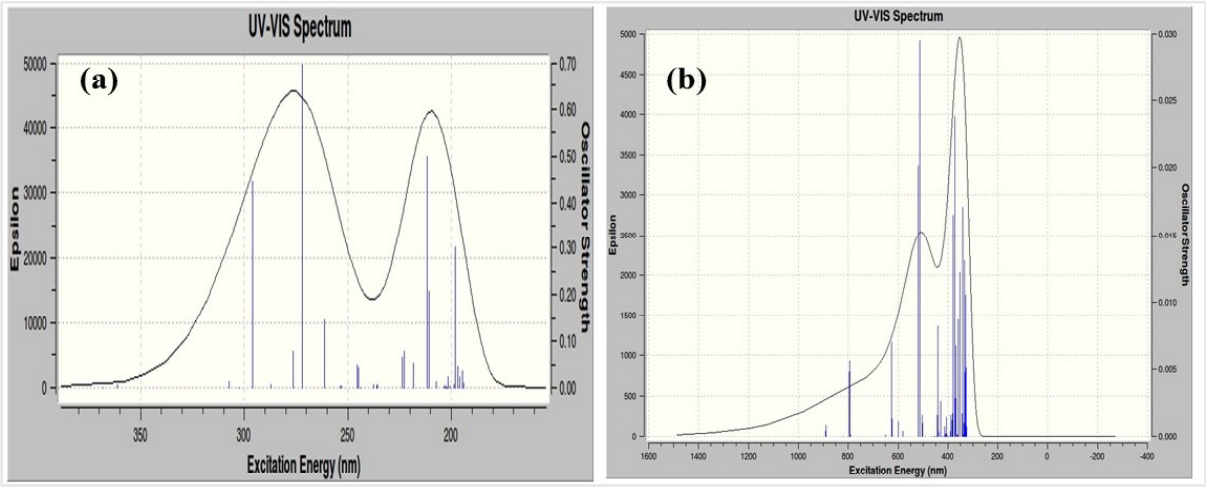

Figure 4B.12: (a) Theoretical UV-visible spectra of receptor **L2c** and (b) **Fe(II)-L2c** complex

4B.3.9 Real Time Application

River water analysis was performed to check the matrix effect on the receptor of **L2c**. Complexation (**L2c**: Fe^{+2}) titrations were carried out in river water and triple distilled water, respectively. The river water system could not affect the detection of spiked Fe^{+2} ion. Figure 4B.13 shows the peak pattern of **Fe(II)–L2c** complex in an isolated matrix system of river water. Table 4B.3 represents the variation of spiked metal ion concentration into the river water and found metal ion concentration which was calculated from the calibration plot (Complexation titration in triple distilled water).

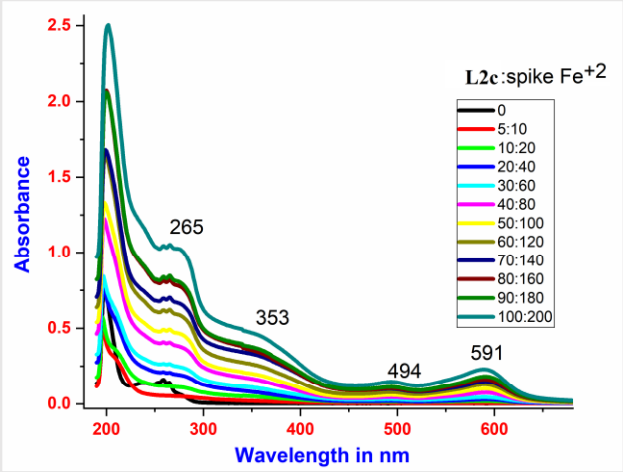

Figure 4B.13: The UV-visible spectra represents the determination of spike Fe(II) ion in river water sample by **L2c**

Table 4B.3: Spike Fe(II) ion determination in river water

River water (mL)	Added µM	Found µM	RSD
1	10	13.15	30.17
1	20	16.23	8.78
1	30	20.0	7.86
1	40	27.75	2.88
1	50	34.69	3.43
1	60	41.98	1.84
1	70	46.85	2.23
1	80	50.36	1.93
1	90	55.31	2.67
1	100	67.29	0.52

4B.4 Conclusion

From a synthesis point of view, our receptor (bis(pyridyl)-ethylene-di-imines) is simple molecule when compared to other iron sensors. Selectively, Fe^{+2} is detected at 595 nm with hump 507 nm in UV-visible region with a distinguished peak 372 nm by receptor **L2c**, in 1:2 ratio (**L2c**: Fe^{+2}) complex formation having detection limit 25µM. In the naked eye, Fe^{+2} can recognize with dark purple colour even up to micromolar level. For our clarification, various Fe^{+3} salts were taken to record the UV-visible spectra to check the instant complex formation, but it could not detect any peak around the UV-visible region. The larger HOMO-LUMO gap of the receptor is an ideal donor to form complexation with Fe(II) system. The TD-DFT data of electronic absorption spectra showed good agreement with the experimental UV-visible spectra. The fluorescent receptor of **L2c** could act as a sensor for Fe(II) in an environmental sample in pH 5-10. Comparison of other reported sensors were listed in Table A-8a. The

analysis of PL spectra also revealed that the receptor was a turn off fluorescence for Fe^{+2} over other metal ions. **L2c** could be explored as faster colorimetric fluorescence off probe for Fe(II) in presence of other competitive metal ions.

4B.5 References

[1] Tchounwou P. B., Yedjou C. G., Patlolla A. K., Sutton D. J., *Molecular, Clinical and Environmental Toxicology: Volume 3: Environmental Toxicology*. Springer Basel; **2012**:133-164.

[2] (a) Pal S., Chatterjee N., Bharadwaj P. K., *RSC Adv.,* **2014**, 4(51), 26585-26620; (b) Chowdhury S., Rooj B., Dutta A., Mandal U., *J. Fluoresc.,* **2018**, 28(4), 999-1021; (c) Breuer W., Epsztejn S., Millgram P., Cabantchik I. Z., *Am. J. Physiol. Cell Physiol.,* **1995**, 268(6), C1354-C1361.

[3] Kobayashi T., Nishizawa N. K., *Plant Sci.,* **2014**, 224, 36-43.

[4] (a) Wu D., Sedgwick A. C., Gunnlaugsson T., Akkaya E. U., Yoon J., James T. D., *Chem. Soc. Rev.,* **2017**, 46(23), 7105-7123; (b) Suganya S., Naha S., Velmathi S., *ChemistrySelect,* **2018**, 3(25), 7231-7268.

[5] Aron A. T., Reeves A. G., Chang C. J., *Curr. Opin. Chem. Biol.,* **2018**, 43, 113-118.

[6] Wan C.-F., Chang Y.-J., Chien C.-Y., Sie Y.-W., Hu C.-H., Wu A.-T., *J. Lumin.,* **2016**, 178, 115-120.

[7] Choi Y. W., Park G. J., Na Y. J., Jo H. Y., Lee S. A., You G. R., Kim C., *Sens. Actuators, B,* **2014**, 194, 343-352.

[8] You G. R., Park G. J., Lee S. A., Ryu K. Y., Kim C., *Sens. Actuators, B,* **2015**, 215, 188-195.

[9] Tang T., Hao Z., Yang H., Nie F., Zhang W., *J. Electroanal. Chem.,* **2020**, 856, 113498.

[10] Samadi-Maybodi A., Rezaei V., Rastegarzadeh S., *Spectrochim. Acta, Part A,* **2015**, 136, 832-837.

[11] Hassan H. M. A., Shahat A., Azzazy H. M. E., El-aal R. M. A., El-Sayed W. N., Elwahed A. A., Awual M. R., *Microchem. J.,* **2020**, 154, 104578.

[12] Au-Yeung H. Y., Chan J., Chantarojsiri T., Chang C. J., *J. Am. Chem. Soc.,* **2013**, 135(40), 15165-15173.

[13] PETRAT F., de GROOT H., RAUEN U., *Biochem. J,* **2001**, 356(1), 61-69.

[14] Hirayama T., Okuda K., Nagasawa H., *Chem. Sci.,* **2013**, 4(3), 1250-1256.

[15] Li P., Fang L., Zhou H., Zhang W., Wang X., Li N., Zhong H., Tang B., *Chem. Eur. J.,* **2011**, 17(38), 10520-10523.

[16] Hasinoff B. B., *J. Inorg. Biochem.,* **2003**, 95(2-3), 157-164.

[17] Ali A., Zhang Q., Dai J., Huang X., *Biometals,* **2003**, 16(2), 285-293.

[18] Parsaee Z., Joukar Bahaderani E., Afandak A., *Ultrason. Sonochem.,* **2018**, 40, 629-643.

[19] García-López M. C., Munoz-Flores B. M., Chan-Navarro R., Jiménez-Pérez V. M., Moggio I., Arias E., Rodríguez-Ortega A., Ochoa M. E., *J. Organomet. Chem.,* **2016**, 806, 68-76.

[20] Arroudj S., Bouchouit M., Bouchouit K., Bouraiou A., Messaadia L., Kulyk B., Figa V., Bouacida S., Sofiani Z., Taboukhat S., *Opt. Mater.,* **2016**, 56, 116-120.

[21] El-Mossalamy E., Aal S. A., El-Batouti M., Al-Harbi N., *Asian J. Chem.,* **2016**, 28(5), 947.

[22] Tanak H., *Mol. Phys.,* **2014**, 112(11), 1553-1565.

[23] Rastogi R. B., Jaiswal V., Maurya J. L., *P I MECH ENG J-J ENG,* **2014**, 228(2), 198-205.

[24] (a) Abdel Aziz A. A., Seda S. H., Mohammed S. F., *Sens. Actuators, B,* **2016**, 223, 566-575; (b) Wada M., Sakurai M., Inoue Y., Tamura Y., Watanabe Y., *Magn. Reson. Chem.,* **1995**, 33(6), 453-457; (c) Frischmann P. D., Facey G. A., Ghi P. Y., Gallant A. J., Bryce D. L., Lelj F., MacLachlan M. J., *J. Am. Chem. Soc.,* **2010**, 132(11), 3893-3908; (d) Ghassemzadeh M., Firouzi R., Shirkhani S., Amiri S., Neumueller B., *Polyhedron,* **2014**, 69, 188-196; (e) Paul M. K., Singh Y. D., Dey A., Saha S. K., Anwar S., Chattopadhyay A. P., *Liq. Cryst.,* **2016**, 43(3), 343-360; (f) Tang H.-H., Zhang L., Zeng L.-L., Fang X.-M., Lin L.-R., Zhang H., *RSC Adv.,* **2015**, 5(46), 36813-36819; (g) Fukui K., *Angew. Chem., Int. Ed. Engl.,* **1982**, 21(11), 801-809.

[25] Reffas H., Benabdallah T., Al-Taiar A., Hadj Youcef M., *Phys. Chem. Liq.,* **2007**, 45(6), 641-648.

[26] (a) Shiri-Yekta Z., Zamani A., Yaftian M., *Sep. Purif. Technol.,* **2009**, 66(1), 98-103; (b) Oshima S., Kubono K., Kokusen H., Komatsu Y., Hirayama N., *J. Ion Exch.,* **2007**, 18(4), 364-369.

[27] Das M., Baig F., Sarkar M., *RSC Adv.,* **2016**, 6(63), 57780-57792.

[28] Das M., Sarkar M., *ChemistrySelect,* **2019**, 4(2), 681-692.

[29] Dong Y.-B., Smith M. D., zur Loye H.-C., *Inorg. Chem.,* **2000**, 39(21), 4927-4935.